Rapidity spectra of the secondaries produced in heavy ion collisions and the constituent picture of the particles

Bhaskar De*
Institute of Mathematical Sciences, C.I.T. Campus, Taramani, Chennai 600113, India

S. Bhattacharyya†
Physics and Applied Mathematics Unit (PAMU), Indian Statistical Institute, Kolkata 700108, India
(Received 8 March 2004; published 17 February 2005)

The present study is both a reanalysis and an extension of the approach initiated by S. Eremin and S. Voloshin [Phys. Rev. C, **67**, 064905 (2003)]. We attempt to interpret here the rapidity spectra of the various particles produced in both Pb + Pb and Au + Au collisions at SPS-CERN (Super Proton Synchrotron at Conseil Européen pour la Recherche Nucléaire) and RHIC-BNL (Relativistic Heavy Ion Collider at Brookhaven National Laboratory). The study made here is wider in scope and is more species specific than earlier ones, and the results obtained here are compared with those found in previous works based on HIJING, VENUS, etc., at various centralities. The study reconfirms that the constituent parton picture of the particles provides a better and more unified description of the rapidity-density yields for the various secondaries, including some light cluster particles such as deuteron, even in heavy ion collisions.

DOI: 10.1103/PhysRevC.71.024903 PACS number(s): 25.75.−q

I. INTRODUCTION

Recently, Eremin and Voloshin [1] proposed that both nucleons and individual nuclei could be considered to be superpositions of the constituents (of the particles) called partons/quarks/valons, etc. Normally it is assumed that the nucleons are built of three such constituent partons and that the mesons are composed of two of them. Such a constituent picture helps us to interpret the deep inelastic collision processes involving lepton-hadron, hadron-hadron, and hadron-nucleus collisions. Much earlier, Bialas *et al*., within the framework of the additive quark model (AQM) [2], explored the hypothesis that the constituent partons(quarks) provide the universal elements not only of nucleon-nucleon and nucleon-nucleus reactions but also of nucleus-nucleus interactions at high energies; this study showed clear evidence of this possibility. But because the focus was on different issues, the central theme of that work deviates from that of the present work. We simply look into the behavior of some chosen observables for nucleus-nucleus collisions alone, from the viewpoint of such a partonic constituent picture. The centrality dependence of multiplicity density offers a very fundamental observable, and we present here our studies on production of pions, kaons, protons, and antiprotons separately in both Pb + Pb (including deuteron production for this collision) at SPS-CERN (Super Proton Synchrotron at Conseil Européen pour la Recherche Nucléaire), and Au + Au collisions at RHIC-BNL (Relativistic Heavy Ion Collider at Brookhaven National Laboratory) at $\sqrt{s_{NN}} = 130$ and 200 GeV, respectively. Data on deuteron production in the Pb + Pb collision have been obtained very recently and are also taken into account here. Aside from this, we compare the performance of the present approach with that obtained on the basis of some standard programs such as HIJING, VENUS, etc., which are essentially much more complicated than the one dealt with here. Our objective here is to examine the efficacy of this approach in explaining some relevant data on production of these very important kinds of secondaries in the few now-available high energy nuclear collisions. The approach was also successfully tested for production of neutral particles, such as photons, by Netrakanti and Mohanty [3] very recently and was found to be in accord with the contention of Eremin and Voloshin [1].

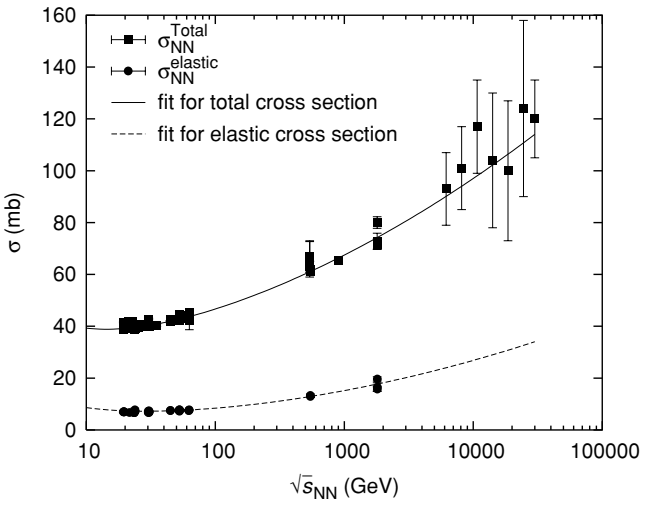

FIG. 1. Plots of total and elastic cross sections of PP and $P\bar{P}$ interactions as a function of c.m. energies. Data points are taken from Ref. [6]. The solid curve depicts the fit for total cross sections on the basis of Eq. (3); the dashed curve is for elastic cross sections on the basis of Eq. (4).

*E-mail address: bhaskar@imsc.res.in.
†Corresponding author; E-mail address: bsubrata@isical.ac.in.

TABLE I. Values of inelastic nucleon-nucleon cross sections at different energies. The second column provides the values obtained by subtracting Eq. (4) from Eq. (3). The last column gives the values as cited in Ref. [5].

$\sqrt{s_{NN}}$ (GeV)	$\sigma_{NN}^{\text{inel}}$ (mb) (Present work)	$\sigma_{NN}^{\text{inel}}$ (mb) (From Ref. [5])
53	35	–
56	35	37
130	40	41
200	42	42
540	48	–
630	49	–
900	51	–
1800	56	–

II. THE OUTLINE OF THE CALCULATION OF THE NUMBER OF PARTICIPANTS

In calculating the number of participant nucleons, denoted by $N_{n\text{-part}}$, and the number of participant partons, denoted by $N_{q\text{-part}}$ we follow exactly the methods adopted by Eremin and Voloshin [1] and Netrakanti and Mohanty [3], wherein a Woods-Saxon nuclear density profile is taken into account. This is given by

$$n_A(r) = \frac{n_0}{1 + \exp[(r - R)/d]}, \tag{1}$$

where $n_0 = 0.17$ fm^{-3}, $R = (1.12A^{1/3} - 0.86A^{-1/3})$ fm, and $d = 0.54$ fm.

The number of participant nucleons ($N_{n\text{-part}}$) for a nucleus-nucleus ($A + B$) collision at an impact parameter b is calculated using the expression [1,3]

$$N_{n\text{-part}}|_{AB} = \int d^2s\, T_A(\vec{s}) \left\{ 1 - \left[1 - \frac{\sigma_{NN}^{\text{inel}} T_B(\vec{s} - \vec{b})}{B} \right]^B \right\} + \int d^2s\, T_B(\vec{s} - \vec{b}) \left\{ 1 - \left[1 - \frac{\sigma_{NN}^{\text{inel}} T_A(\vec{s})}{A} \right]^A \right\}, \tag{2}$$

where A and B are the mass numbers of the two colliding nuclei, $T(b) = \int_{-\infty}^{\infty} dz\, n_A(\sqrt{b^2 + z^2})$ is the thickness function, and $\sigma_{NN}^{\text{inel}}$ is the inelastic nucleon-nucleon cross section. The number of participant partons is also calculated in a similar manner by taking into account the following changes related to physical realities: (i) the density is three times that of the nucleon density with $n_0^q = 3n_0 = 0.51$ fm^{-3}; (ii) the cross sections are $\sigma_{qq} = \sigma_{NN}^{\text{inel}}/9$; and (iii) the mass

TABLE II. Values of $\langle N_{n\text{-part}} \rangle$ and $\langle N_{q\text{-part}} \rangle$ for Pb + Pb collisions at $E_{\text{Lab}} = 158$ A GeV.

Centrality (%)	$\langle N_{n\text{-part}}^{\text{NA49}} \rangle$ [8]	$\langle N_{n\text{-part}}^{\text{Present work}} \rangle$	$\langle N_{q\text{-part}}^{\text{Present work}} \rangle$
0–5	362	368	856
5–14	305	290	644
14–23	242	210	446
23–32	189	140	278
32–47	130	92	171
47–99	72	32	53
Centrality (%)	$\langle N_{n\text{-part}}^{\text{WA98}} \rangle$ [9]	$\langle N_{n\text{-part}}^{\text{Present work}} \rangle$	$\langle N_{q\text{-part}}^{\text{Present work}} \rangle$
0–1	380 ± 1	385	901
1–6.8	346 ± 1	338	770
6.8–13	290 ± 2	273	600
13–25.3	224 ± 1	196	411
25.3–48.8	132 ± 3	99	189
48.8–67	63 ± 2	35	56
67–82.8	30 ± 2	10	14
82.8–100	12 ± 2	3	4

TABLE III. Values of $\langle N_{n\text{-part}} \rangle$ and $\langle N_{q\text{-part}} \rangle$ for Au + Au collisions at $\sqrt{s_{NN}} = 130$ GeV.

Centrality (%)	$\langle N_{n\text{-part}}^{\text{PHENIX}} \rangle$ [10,11]	$\langle N_{n\text{-part}}^{\text{Present work}} \rangle$	$\langle N_{q\text{-part}}^{\text{Present work}} \rangle$
0–5	347.7 ± 10	351	880
5–10	293 ± 10	297	710.6
5–15	271.3 ± 8.4	272	645
10–15	248 ± 8	242.5	565.4
15–20	211 ± 7	207	469.4
20–25	177 ± 7	173	381
15–30	180.2 ± 6.6	174.5	387.3
25–30	146 ± 6	139	298
30–35	122 ± 5	120	249
35–40	99 ± 5	96	192
40–45	82 ± 5	81.5	158.7
45–50	68 ± 4	62	114.6
30–60	78.5 ± 4.6	77	150.1
60–92	14.3 ± 3.3	11.8	17.8

TABLE IV. Values of $\langle N_{n\text{-part}} \rangle$ and $\langle N_{q\text{-part}} \rangle$ for Au + Au collisions at $\sqrt{s_{NN}} = 200$ GeV.

Centrality (%)	$\langle N_{n\text{-part}}^{\text{PHENIX}} \rangle$ [12]	$\langle N_{n\text{-part}}^{\text{Present work}} \rangle$	$\langle N_{q\text{-part}}^{\text{Present work}} \rangle$
0–5	351.4 ± 2.9	351.9	880.1
0–10	325.2 ± 3.3	332.5	819.7
5–10	299.0 ± 3.8	292.2	694.6
10–15	253.9 ± 4.3	242.4	560.9
10–20	234.6 ± 4.7	226.2	517.4
15–20	215.3 ± 5.3	208.2	469
20–30	166.6 ± 5.4	157	339
30–40	114.2 ± 4.4	108.4	218
40–50	74.4 ± 3.8	71.5	134.3
50–60	45.5 ± 3.3	40.4	68.8
60–70	25.7 ± 3.8	23	35.6
60–80	19.5 ± 3.3	16.6	25
60–92	14.5 ± 2.5	11.8	17.3
70–80	13.4 ± 3.0	9.9	13.6
70–92	9.5 ± 1.9	6.8	9.1
80–92	6.3 ± 1.2	3.9	5

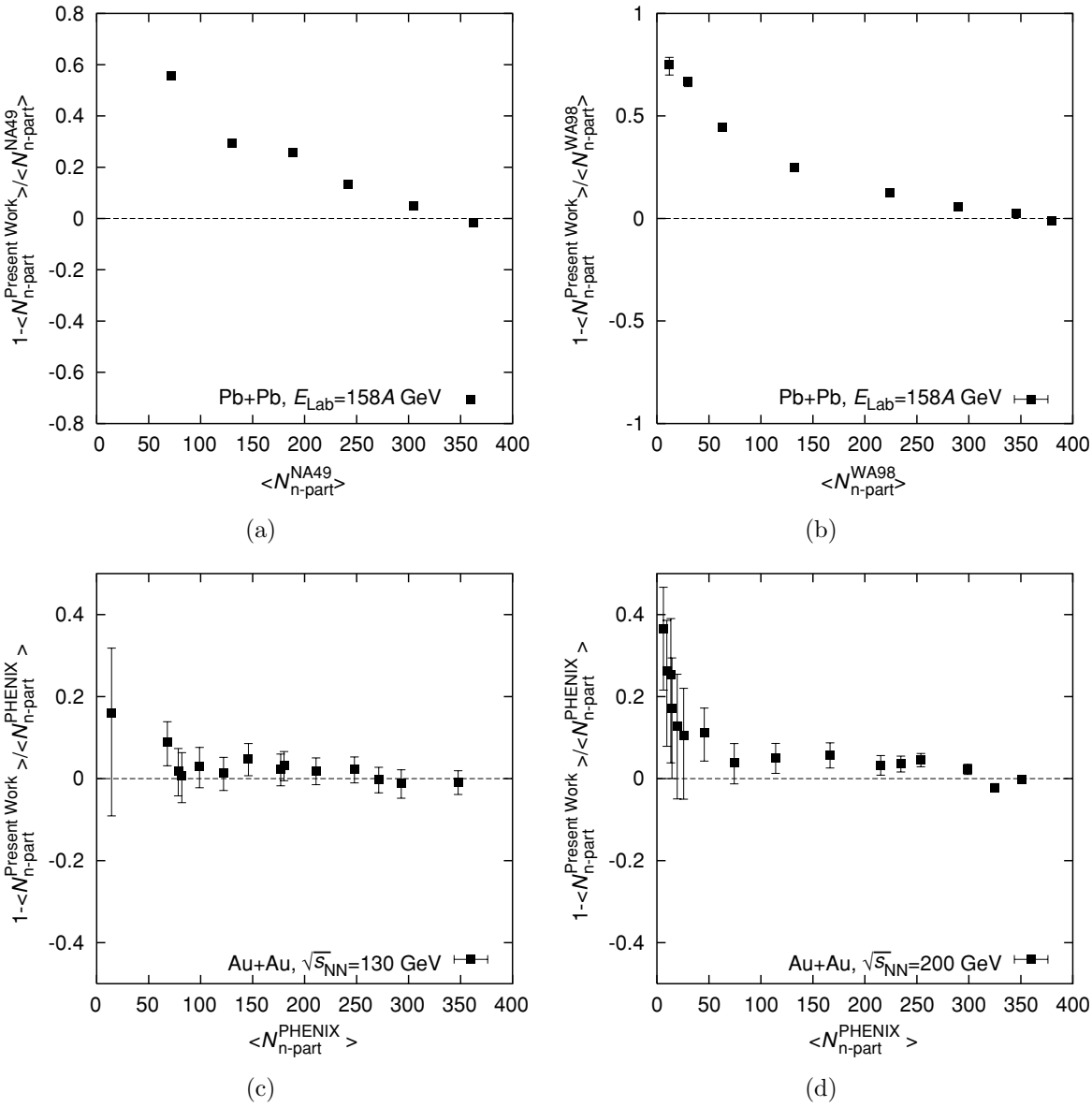

FIG. 2. Comparison of average number of participant nucleons obtained in the present work and in different experimental collaborations in various heavy ion collisions. The experimental data are taken from Refs. [8–12].

numbers of the colliding nuclei are three times their values, keeping the size of the nuclei same as in the case of the $N_{n\text{-part}}$ [1,3].

In the same way, the number of participant partons in a PP or $P\bar{P}$ collision can also be calculated by using $A = 3$ and $B = 3$ and considering nucleons as hard spheres of uniform radii 0.8 fm [4].

For the present work, we use $\sigma_{NN}^{\text{inel}} = 30$ mb in the range of c.m. energies $\sqrt{s_{NN}} = 4$–17.3 GeV as suggested in Ref. [5]. For higher energies, we first fit the data on total cross sections for PP and $P\bar{P}$ collisions [6] at energies beyond $\sqrt{s_{NN}} = 30$ GeV with the expression [7]

$$\sigma_{NN}^{\text{total}} = (29.2 \pm 0.3)\left[1 + \frac{(2.2 \pm 0.5)\ \text{GeV}}{\sqrt{s_{NN}}}\right] + (1.1 \pm 0.1) \times \ln\left(\frac{s_{NN}}{10\ \text{GeV}^2}\right) + (0.19 \pm 0.01)\ln^2\left(\frac{s_{NN}}{10\ \text{GeV}^2}\right) \quad (3)$$

with $\chi^2/\text{ndf} = 171/47$, where ndf = number of data points-number of parameters. We also fit the elastic cross-section data for the same interactions [6] with a similar type of expression, which is given by

$$\sigma_{NN}^{\text{elastic}} = (6.2 \pm 0.2)\left[1 + \frac{(4.8 \pm 1.4)\ \text{GeV}}{\sqrt{s_{NN}}}\right] - (0.47 \pm 0.04) \times \ln\left(\frac{s_{NN}}{10\ \text{GeV}^2}\right) + (0.11 \pm 0.01)\ln^2\left(\frac{s_{NN}}{10\ \text{GeV}^2}\right) \quad (4)$$

with $\chi^2/\text{ndf} = 53.14/18$. The fits, along with the data, are shown in Fig. 1. Hence, one can obtain the energy dependence of the inelastic cross section ($\sigma_{NN}^{\text{inel}}$) for nucleon-nucleon interaction by subtracting Eq. (4) from Eq. (3). The values of $\sigma_{NN}^{\text{inel}}$ obtained in this manner, at some energies, are given in Table I. The obtained values fall within a 6% error range of

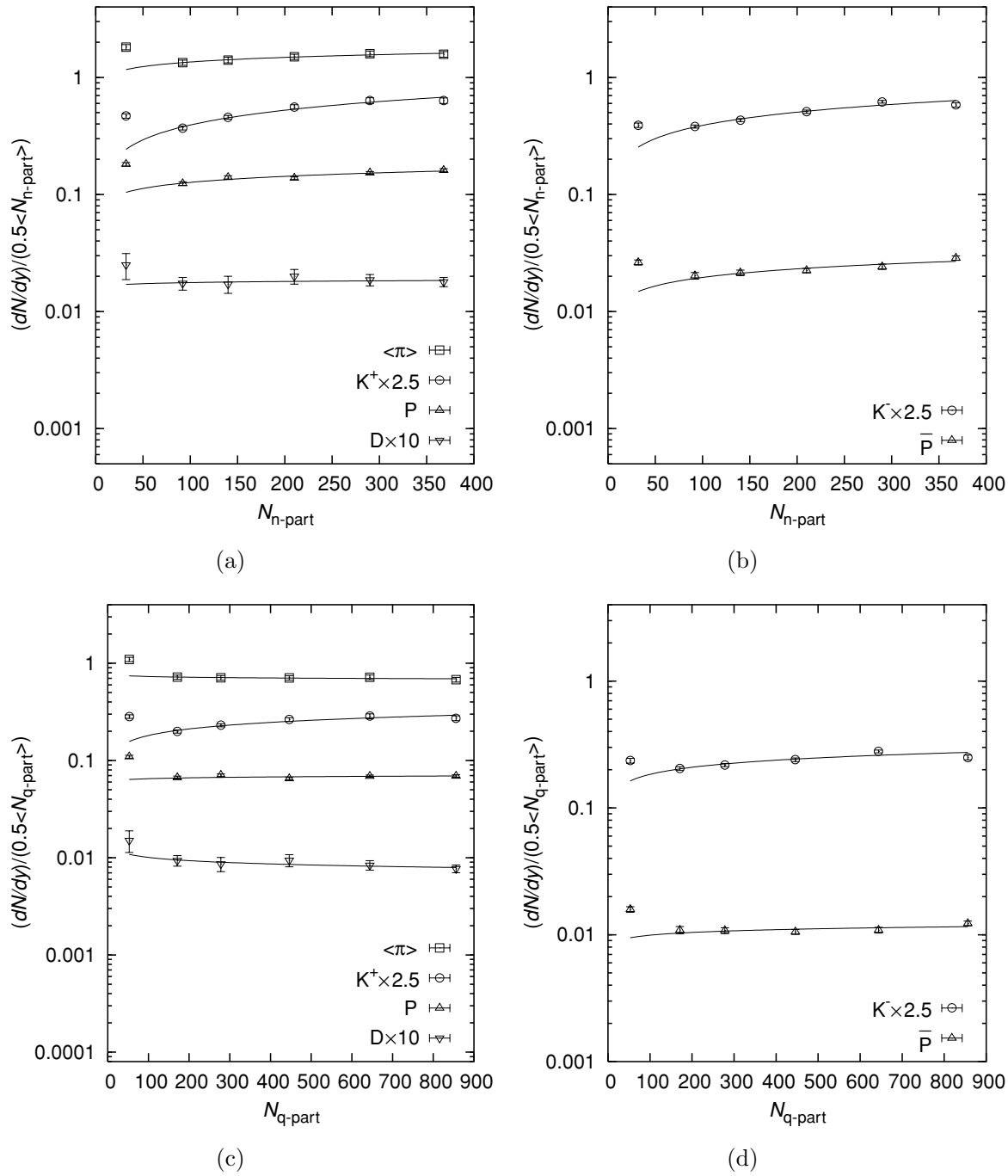

FIG. 3. Plots of integrated yields normalized by half of the number of participant nucleons [(a) and (b)] or constituent partons [(c) and (d)] as a function of centralities for production of the various identified secondaries in Pb + Pb collisions at $E_{\rm Lab} = 158\,A$ GeV [8,17]. The curves represent the fits obtained on the basis of Eqs. (5) [(a) and (b)] and (6) [(c) and (d)].

those suggested in Ref. [5]. But a point is to be noted. Although there is some justification for proposing the nature of the total cross section in the form of expression (3) given in Ref. [7], no such explanation for expression (4) is possible. This is simply assumed, with a view to providing only a best fit to the available data on the elastic cross section shown in Fig. 1 and extracting a workable phenomenological form of expression for the nature of the inelastic cross section $\sigma_{NN}^{\rm inel}$. In fact, these twin relations help us to arrive at the usable values of inelastic cross sections needed to carry out our necessary calculations of the relevant observables in a systematic manner, even at energies for which no measured data on cross section values are available.

III. RESULTS AND DISCUSSION

The values of the number of participant nucleons and those of the participant partons for three nucleus-nucleus collisions

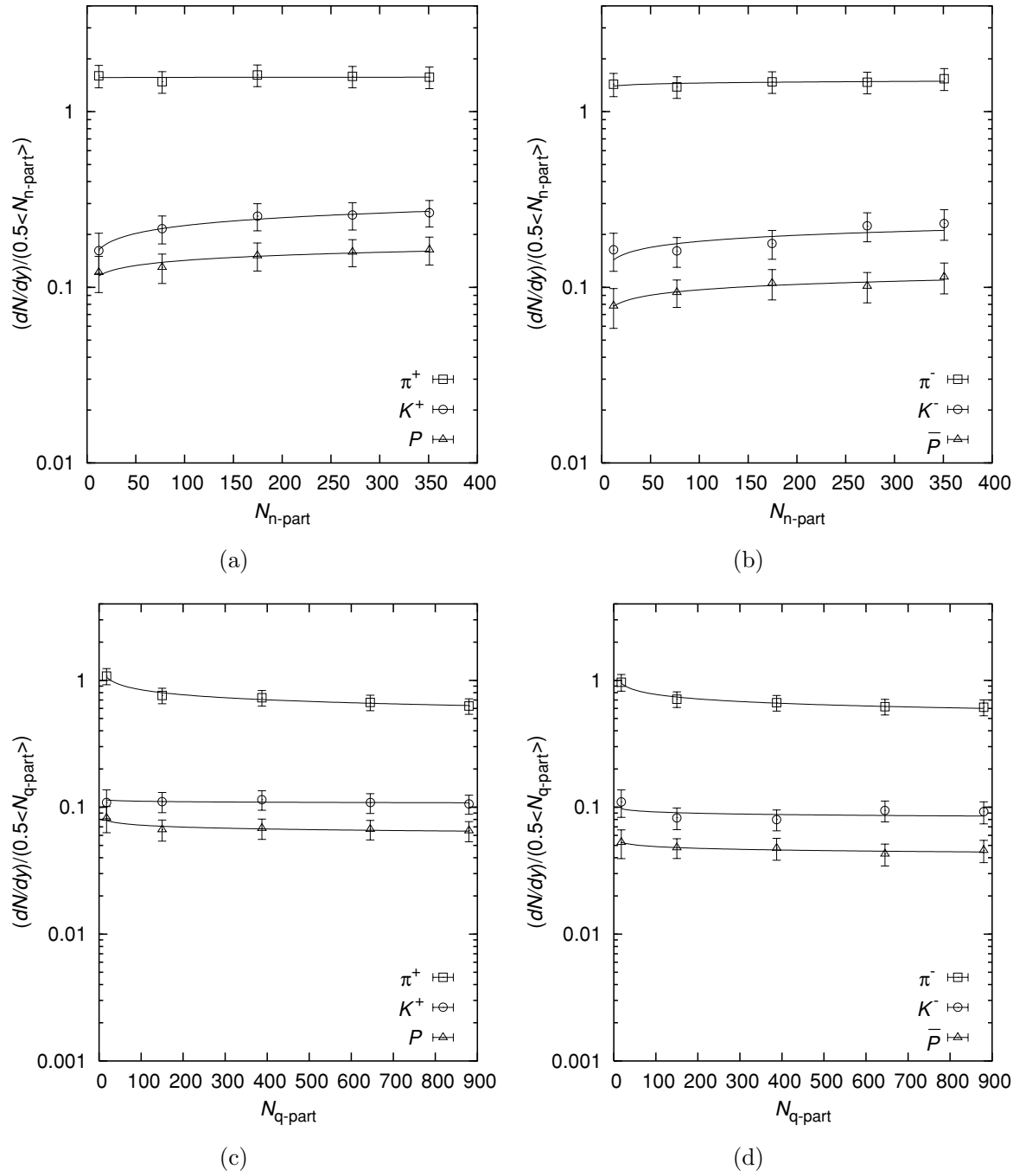

FIG. 4. Plots of integrated yields normalized by half of the number of participant nucleons [(a) and (b)] or constituent partons [(c) and (d)] as a function of centralities for production of the various identified secondaries in Au + Au collisions at $\sqrt{s_{NN}} = 130$ GeV [10]. The curves represent the fits obtained on the basis of Eqs. (5) [(a) and (b)] and (6) [(c) and (d)].

at various energies and different centralities are presented in Tables II–IV. A comparison of the results obtained on the basis of the present work with those of the NA49 [8], WA98 [9], and PHENIX [10–12] groups is made in Figs. 2(a)–(d), in terms of $1 - \frac{\langle N_{n\text{-part}}^{\text{Present work}} \rangle}{\langle N_{n\text{-part}}^{\text{NA49/WA98/PHENIX}} \rangle}$ versus $N_{n\text{-part}}^{\text{NA49/WA98/PHENIX}}$. It is observed that the agreements in cases of Au + Au collisions are modestly fair, whereas for Pb + Pb interaction the disagreement is quite strong and prominent. This discrepancy could, for the present, be attributed to the much lower c.m. energy in the lead-lead reaction, which falls roughly at only 17.2 GeV.

The integrated yields of the identified hadrons at the central rapidity region produced in Pb + Pb and Au + Au collisions at different centralities are presented diagrammatically in Figs. 3–5. In parts (a) and (b) of each figure, the experimental data on integrated yields ($\frac{dN}{dy}$) are normalized by half of the number of participant nucleons ($N_{n\text{-part}}$), and those in parts (c) and (d) are normalized by half of the number of participant

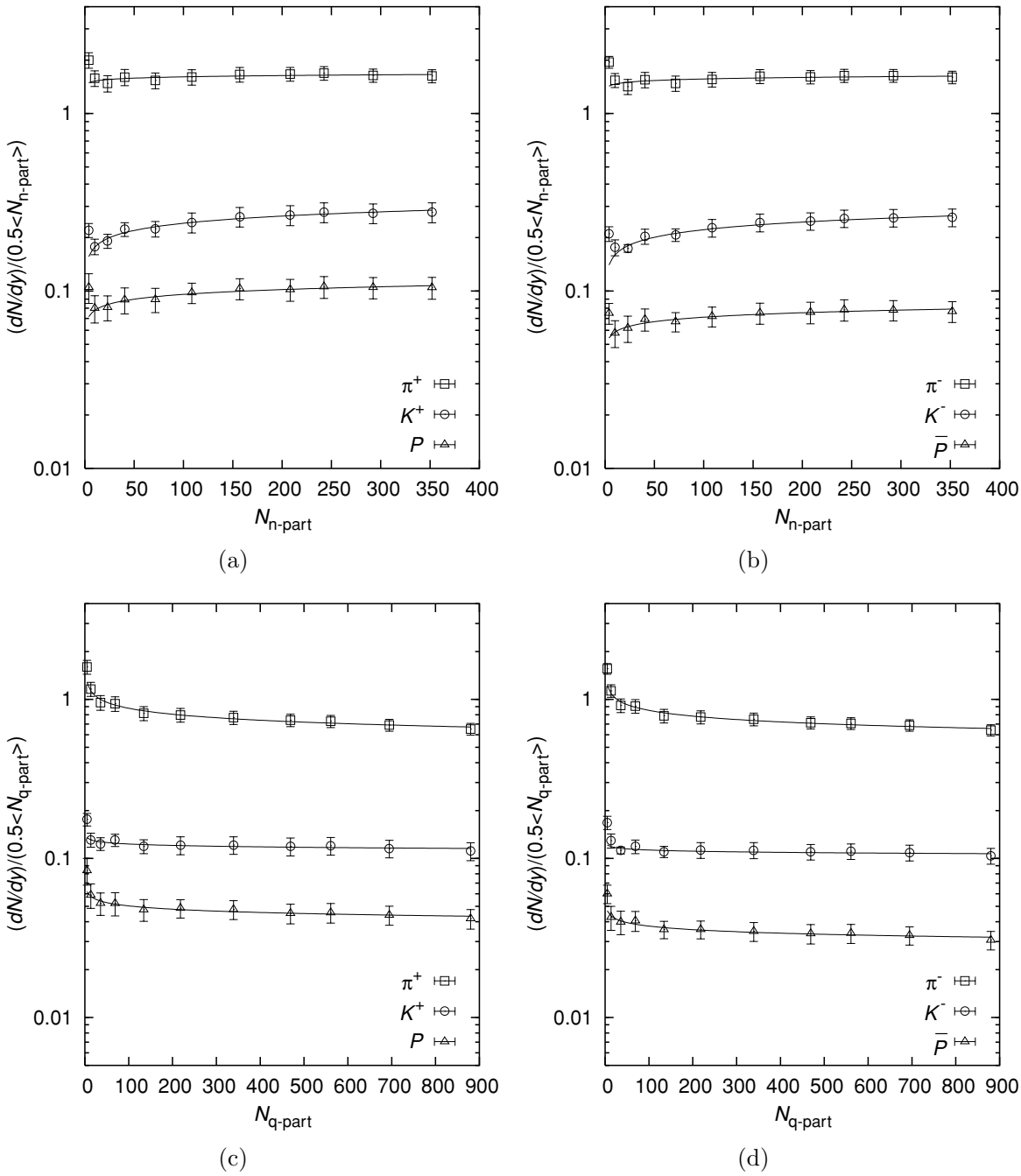

FIG. 5. Plots of integrated yields normalized by half of the number of participant nucleons [(a) and (b)] or constituent partons [(c) and (d)] as a function of centralities for production of the various identified secondaries in Au + Au collisions at $\sqrt{s_{NN}} = 200$ GeV [12]. The curves represent the fits obtained on the basis of Eqs. (5) [(a) and (b)] and (6) [(c) and (d)].

partons ($N_{q\text{-part}}$). Since we are comparing these two cases, we should use values of both the observables obtained from a single model. That is why we put into use the values of $\langle N_{n\text{-part}}\rangle$ obtained on the basis of the present work, instead of the values indicated by the NA49 [8] or PHENIX groups [10–12].

Now, to make a comparison between these two cases, we fit the data in Figs. 3–5 by two phenomenological expressions, which are given by

$$\frac{1}{0.5\langle N_{n\text{-part}}\rangle}\frac{dN}{dy} = aN_{n\text{-part}}^{\alpha} \tag{5}$$

and

$$\frac{1}{0.5\langle N_{q\text{-part}}\rangle}\frac{dN}{dy} = bN_{q\text{-part}}^{\beta}, \tag{6}$$

where a, b, α, and β are four constants. The fitted values of these parameters are given in Tables V–VII and depicted by solid curves in the figures. As can be seen from Figs. 2(a), (b), and (d), the most peripheral values of $N_{n\text{-part}}$ for Pb + Pb collision at $E_{\text{Lab}} = 158\,A$ GeV and Au + Au collision at $\sqrt{s_{NN}} = 200\,\text{GeV}$ obtained by the present model show larger

discrepancies with respect to those obtained by the NA49 and PHENIX collaborations. Therefore, we keep most peripheral data in these two collisions out of the range of both the fits provided by Eqs. (5) and (6).

Obviously, the factors α and β provide the slopes of the fits. As the magnitude of any of these factors becomes closer to zero, the fit will exhibit better flatness of the data with respect to $N_{n\text{-part}}$ or $N_{q\text{-part}}$, implying a superior compliance of scaling, i.e., a better scaling. A look at Table V reveals that the data on $\langle\pi\rangle$, $K^{\pm}$, and $P/\bar{P}$ in Pb + Pb collisions show a better degree of conformity with scaling when normalized by half of $N_{q\text{-part}}$, as in all cases $|\beta|$ is less than $|\alpha|$. But, for the case of deuteron production in Pb + Pb collision, the scenario is just the opposite. Besides, the integrated yields for charged pions produced in Au + Au interactions at both the RHIC energies (Tables VI and VII) do not exhibit scaling satisfactorily when the data are normalized by half of $N_{q\text{-part}}$ instead of $N_{n\text{-part}}$, as the values of $|\alpha|$, in these cases, are quite small with respect to $|\beta|$. However, the data on $K^{\pm}$ and $P/\bar{P}$ produced in the same collisions favor the $N_{q\text{-part}}$ scaling over the $N_{n\text{-part}}$ scaling, though the cases of $P/\bar{P}$ at $\sqrt{s_{NN}} = 200$ GeV are not as prominent as they are at other values. In summary, our net finding from the present study is that the pions do not agree, whereas the kaons and protons do.

Figure 6(a) deserves some special attention and comment. The plots on integrated yields for charged hadrons produced in both nucleus-nucleus ($A + A$) and $P + \bar{P}$ collision deflect from each other when data on both are separately normalized in terms of the number of participating nucleons ($N_{n\text{-part}}$). The data on integrated yields in central nucleus-nucleus collisions normalized by the number of participant nucleon pairs have been used here from Fig. 3 of Ref. [13]. For our purposes, this has to be normalized in terms of the basic parton(quark) constituents, denoted by $\langle N_{q\text{-part}}\rangle$, for which the (charged)pseudo-rapidity density terms for various nucleus-nucleus collisions normalized by participant nucleon pair, i.e., the factors $\frac{1}{0.5\langle N_{n\text{-part}}\rangle}\frac{dN_{\rm ch}}{d\eta}$ are to be multiplied by $R = \langle N_{n\text{-part}}\rangle/\langle N_{q\text{-part}}\rangle$, with the values as given in Table VIII. And, in this conversion we have utilized those particular values of $\langle N_{n\text{-part}}\rangle$ that were used in Ref. [13], so that we can normalize the exact values of $\frac{dN_{\rm ch}}{d\eta}$ by $\langle N_{q\text{-part}}\rangle/2$, where $N_{\rm ch}$ is the multiplicity of the secondary charged hadrons produced in a specific collision. In calculating $N_{q\text{-part}}$ for $P + \bar{P}$ collisions, we use Eq. (2), and the values of $N_{q\text{-part}}$ for $P + \bar{P}$ collisions at three different c.m. energies are given in Table IX as a function of relative probability.

When partonic considerations are used in normalization, the data on both $P + \bar{P}$ and $A + A$ collisions come to an agreeable state. The $\langle N_{q\text{-part}}\rangle$ values that are to be used for normalization of the most central $P + \bar{P}$ collisions, i.e., $0 - 5\%$ central collisions, are depicted in Table X. In order to check the nature of agreement between the data on $A + A$ and $P + \bar{P}$ collisions, we try to obtain a fit by taking into account both sets of data, normalized by $\langle N_{q\text{-part}}\rangle/2$; and the desired fit is to be described here by the expression

$$\frac{1}{0.5\langle N_{q\text{-part}}\rangle}\frac{dN_{\rm ch}}{d\eta} = -(0.010 \pm 0.003) + (0.27 \pm 0.01)\ln\left(\frac{\sqrt{s_{NN}}}{\rm GeV}\right), \quad (7)$$

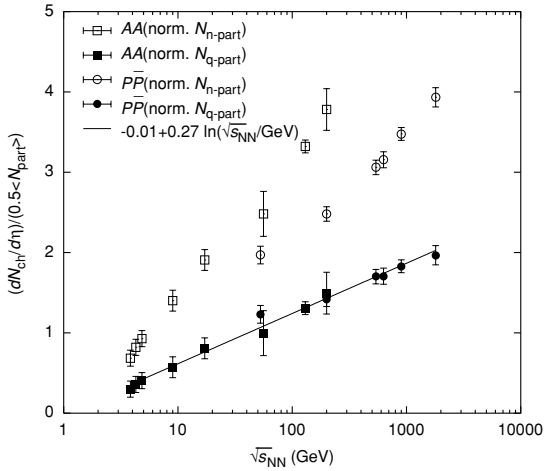

(a)

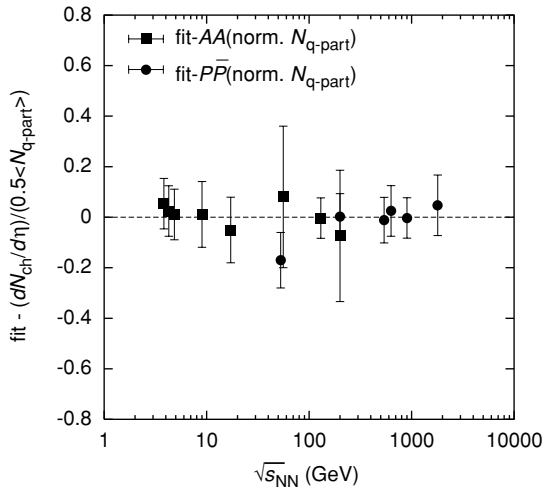

(b)

FIG. 6. (a) Energy dependencies of integrated yields for charged hadrons produced in different nucleus-nucleus ($A + A$) collisions at Alternating Gradient Synchrotron (AGS), SPS, and RHIC energies and in $P + \bar{P}$ collisions at Intersecting Storage Ring (ISR) energies (Fig. 3 of Ref. [13]). The open boxes and open circles provide the data normalized by half of the average number of participant nucleons for nucleus-nucleus and $P\bar{P}$ collisions, respectively. The solid boxes and solid circles show the same result for $A + A$ and $P + \bar{P}$ collisions normalized by half of the number of the participant partons. The solid line provides a fit [Eq. (7)] for the nucleus-nucleus and proton-antiproton data normalized by half of the corresponding average number of constituent partons. (b) The plot of closeness of the different sets of data with respect to the aforementioned fit.

with $\chi^2/\text{ndf} = 3.632/12$. The goodness of the fit is also shown in Fig. 6(b) with the help of the expression *fit-data* as a function of $\sqrt{s_{NN}}$, which reveals that both sets of data are in good agreement with respect to the fit. Hence, both $A + A$ and $P + \bar{P}$ data exhibit a common $\sqrt{s_{NN}}$ dependence when the data on the former are normalized by the number of participant parton pairs.

TABLE V. Values of a, b, α, and β for production of various secondaries in Pb + Pb collisions at $E_{\rm Lab} = 158\,A$ GeV (ndf = number of data points-number of parameters in the fit).

Identified secondary	a	α	χ^2/ndf	b	β	χ^2/ndf
$\langle\pi\rangle$	0.74 ± 0.06	0.13 ± 0.01	0.320/3	0.82 ± 0.08	$-(0.02 \pm 0.01)$	0.442/3
K^+	0.023 ± 0.005	0.42 ± 0.04	3.436/3	0.026 ± 0.006	0.22 ± 0.04	3.700/3
K^-	0.028 ± 0.008	0.37 ± 0.05	11.024/3	0.03 ± 0.01	0.18 ± 0.05	12.514/3
P	0.06 ± 0.01	0.17 ± 0.04	4.492/3	0.06 ± 0.01	0.03 ± 0.01	4.054/3
$\bar{P}$	0.006 ± 0.002	0.24 ± 0.06	4.616/3	0.007 ± 0.002	0.07 ± 0.04	4.313/3
D	0.0015 ± 0.0004	0.05 ± 0.02	0.635/3	0.0017 ± 0.0004	$-(0.11 \pm 0.04)$	0.656/3

TABLE VI. Values of a, b, α, and β for production of various secondaries in Au + Au collisions at $\sqrt{s_{NN}} = 130$ GeV (ndf = number of data points-number of parameters in the fit).

Identified secondary	a	α	χ^2/ndf	b	β	χ^2/ndf
π^+	1.6 ± 0.1	0.0015 ± 0.0003	0.250/3	1.6 ± 0.1	$-(0.13 \pm 0.01)$	0.221/3
π^-	1.3 ± 0.1	0.02 ± 0.01	0.190/3	1.32 ± 0.07	$-(0.12 \pm 0.01)$	0.125/3
K^+	0.11 ± 0.01	0.15 ± 0.01	0.073/3	0.12 ± 0.01	$-(0.012 \pm 0.002)$	0.083/3
K^-	0.11 ± 0.03	0.11 ± 0.06	1.175/3	0.11 ± 0.03	$-(0.03 \pm 0.01)$	1.081/3
P	0.09 ± 0.01	0.10 ± 0.02	0.191/3	0.09 ± 0.01	$-(0.05 \pm 0.01)$	0.151/3
$\bar{P}$	0.06 ± 0.01	0.10 ± 0.02	0.148/3	0.06 ± 0.01	$-(0.04 \pm 0.01)$	0.115/3

TABLE VII. Values of a, b, α, and β for production of various secondaries in Au + Au collisions at $\sqrt{s_{NN}} = 200$ GeV (ndf = number of data points-number of parameters in the fit).

Identified secondary	a	α	χ^2/ndf	b	β	χ^2/ndf
π^+	1.7 ± 0.1	$-(0.008 \pm 0.004)$	4.455/8	1.6 ± 0.1	$-(0.12 \pm 0.01)$	0.769/8
π^-	1.4 ± 0.1	0.03 ± 0.01	1.071/8	1.5 ± 0.1	$-(0.12 \pm 0.01)$	1.015/8
K^+	0.130 ± 0.004	0.13 ± 0.01	0.583/8	0.14 ± 0.01	$-(0.03 \pm 0.01)$	0.591/8
K^-	0.12 ± 0.01	0.14 ± 0.01	1.657/8	0.13 ± 0.01	$-(0.02 \pm 0.01)$	1.490/8
P	0.063 ± 0.002	0.09 ± 0.01	0.264/8	0.069 ± 0.003	$-(0.07 \pm 0.01)$	0.274/8
$\bar{P}$	0.048 ± 0.002	0.08 ± 0.01	0.290/8	0.053 ± 0.002	$-(0.07 \pm 0.01)$	0.347/8

TABLE VIII. Values of $\langle N_{n\text{-part}}\rangle$ and $\langle N_{q\text{-part}}\rangle$ used in Fig. 6(a) to normalize $\frac{dN_{\rm ch}}{d\eta}$ data for various nucleus-nucleus collisions.

Collision type	$\sqrt{s_{NN}}$ (GeV)	Centrality (%)	$\langle N_{n\text{-part}}\rangle$/Ref.	$\langle N_{q\text{-part}}\rangle$
Au + Au	AGS	0–5	343 [14]	786
Pb + Pb	8.7	0–5	349 [15]	856
Pb + Pb	17.2	0–5	362 [15]	856
Au + Au	56	0–6	330 [16]	823
Au + Au	130	0–6	343 [16]	871
Au + Au	200	0–6	344 [13]	871

TABLE IX. Values of $N_{q\text{-part}}$ for proton-antiproton collisions at three different c.m. energies as a function of relative probability.

Relative probability (%)	53 GeV	200 GeV	1800 GeV
0–5	3.2	3.5	4.0
5–10	2.8	3.1	3.7
10–20	2.5	2.8	3.3
20–30	2.1	2.3	2.7
30–40	1.9	2.0	2.5
40–60	1.4	1.5	1.7
60–100	0.9	0.9	1.0

IV. CONCLUDING REMARKS

Let us now summarize our observations: (i) The secondaries, excluding deuterons, produced in Pb + Pb collision at SPS-CERN behave modestly well vis-à-vis $N_{q\text{-part}}$ scaling. The behavior is more consistent towards the highest values of centrality, with a centrality maximum at 0–5% [represented by solid boxes in the graph in Figs. 3(a)–(d)]. (ii) Similar

TABLE X. Values of $\langle N_{q\text{-part}}\rangle$ for most central (0–5%) $P + \bar{P}$ collisions at different c.m. energies.

$\sqrt{s_{NN}}$ (GeV)	53	200	540	630	900	1800
$\langle N_{q\text{-part}}\rangle$	3.2	3.5	3.6	3.7	3.8	4.0

statements can be made about Au + Au interactions at both energies (Figs. 4 and 5), except in the case of pions. (iii) It is quite noticeable that there are modest degrees of divergence in the $N_{n\text{-part}}$ values between the calculations done by us at different centralities and those done by others, as indicated in the text (see the second and third columns of Tables II–IV). For the present, these discrepancies can be attributed only to our computer programs, which are much simpler than those used by the big groups, such as NA49, WA98, PHENIX, etc. The fact is that we are now simply unable to take up such rigorous studies as might be desired or advisable due to various reasons beyond our capacity and control. But we recognize the urgency and importance of such studies in order to arrive at a decision about the merit of $N_{q\text{-part}}$ scaling and the viewpoints expressed by Eremin and Voloshin [1]. (iv) Figure 6 highlights how the data on both $P + \bar{P}$ and $A + A$ collisions better incorporate the idea of partonic-participant scaling when the constituent-participant numbers for both $P + \bar{P}$ and $A + A$ collisions are taken into account. Thus, the present study does provide modest support for the viewpoints expressed by Eremin and Voloshin in Ref. [1].

Note added in proof

While the paper was posted in the archives [nucl-th/0412013] after its acceptance by Physical Review C, Sarkisyan and Sakharov drew our attention to their efforts to fit the observable called rapidity-density in terms of number of participants and the c.m. energy of the collision, within the framework of the Landau model and in a somewhat different perspective. The interested reader might find this work in hep-ph/0410324.

ACKNOWLEDGMENTS

The authors are very grateful to the anonymous referee for his/her very patient readings, constructive criticisms, and kind and valuable instructions for improvements in previous drafts of the manuscript. The authors also express their gratitude to Professor D. Miŝkowiec for providing helpful suggestions about running the FORTRAN code developed by him in calculating the number of participants N_{part}. One of the authors, BD, thanks the IMSc for offering him the support of a postdoctoral Fellowship of the IMSc, wherein a part of this work was done.

[1] S. Eremin and S. Voloshin, Phys. Rev. C **67**, 064905 (2003).
[2] A. Bialas, W. Czyz, and L. Lesniak, Phys. Rev. D **25**, 2328 (1982).
[3] P. K. Netrakanti and B. Mohanty, Phys. Rev. C **70**, 027901 (2004); nucl-ex/0401036.
[4] C. Y. Wong, *Introduction to High-Energy Heavy Ion Collisions* (World Scientific, 1994), p. 161.
[5] D. Miŝkowiec, http://www-linux.gsi.de/∼misko/overlap/manual.ps.
[6] Particle Data Group, http://pdg.lbl.gov/2004/hadronic-xsections/hadron.html.
[7] B. De, S. Bhattacharyya, and P. Guptaroy, J. Phys. G **27**, 2389 (2001).
[8] J. Bachler *et al.* (NA49 Collaboration), Nucl. Phys. **A661** (Suppl. 999), 45c (1999).
[9] M. M. Aggarwal *et al.* (WA98 Collaboration), Eur. Phys. J. C **23**, 225 (2002).
[10] K. Adcox *et al.* (PHENIX Collaboration), Phys. Rev. C **69**, 024904 (2004).
[11] K. Adcox *et al.* (PHENIX Collaboration), Phys. Rev. Lett. **86**, 3500 (2001).
[12] S. Adler *et al.* (PHENIX Collaboration), Phys. Rev. C **69**, 034909 (2004).
[13] B. B. Back *et al.* (PHOBOS Collaboration), Phys. Rev. Lett. **88**, 022302 (2002), and references therein.
[14] J. Klay, Ph.D. thesis, University of California, Davis, 2001, p. 127; http://nuclear.ucdavis.edu/∼jklay/CV/JLK_cv.html.
[15] S. V. Afanasiev *et al.* (NA49 Collaboration), Phys. Rev. C **66**, 054902 (2002).
[16] B. B. Back *et al.* (PHOBOS Collaboration), Phys. Rev. Lett. **85**, 3100 (2000).
[17] T. Anticic *et al.* (NA49 Collaboration), Phys. Rev. C **69**, 024902 (2004).